Modeling and Control of a Hybrid Solar-Wind Power System with Hydrogen Storage

G.B. Hangeragi

Associate Professor, Department of Electronics & Communication,
Bheemanna Khandre institute of Technology Bhalki, Karnataka, INDIA

(Corresponding author: G.B. Hangeragi)

ABSTRACT: This paper deals with system integration and controller design for power management of solar-wind sources energy conversion, system, the system consists of five main components: photovoltaic arrays, wind turbine, electrolyzer, hydrogen storage tanks, and fuel cell. The model for each process component is developed, and all the components are included in a MATLAB/Simulink environment. A two level control system is implemented, first one is a supervisory controller, in this modal, ensures the power balance between intermittent solar / wind energy generation, energy storage, and variable load demand, as well as local controllers for the photovoltaic, wind, electrolyzer, and fuel cell unit. Simulations are performed to document the efficacy of the proposed power management strategy.

I. INTRODUCTION

Renewable energy (RE) (Solar and wind) sources will become an increasingly important part of power generation as the reserves of fossil fuels get closer to depletion. Among them, wind and solar energy sources are the most important options, and is Easily available in nature, freely available, pollution free and environmentally friendly. Although these technologies are improving in various aspects, the drawbacks isa intermittent nature and high investment cost, and utilization their power. As per study result, only 3% of total global electricity is generated from solar/wind renewable sources [1]. Because of their alternating nature, wind and solar energy resources inparticalur given area can be complementary on a daily or seasonal basis.   Its Hybrid combinations for two or more renewable power generation technologies in stand-alone applications are economically viable and can improve the system's performance [2–6]. Additionally, in order to ensure grid-like power for autonomous systems, a storage medium is needed. The energy storage system can be classified on the basis of capacity (i.e. pumped hydroelectric systems, compressed air, hydrogen) and access storage devices (i.e. batteries, flywheels, super capacitors, and superconducting magnetic energy storage) [7].

Each one of them has several advantages and disadvantages and one has to consider factors such as the operating cost, power response time, efficiency and life span when selecting a suitable storage technology. Among them, battery storage is energy efficient, but the cost of energy storage is very high [8]. Pumped hydro is suitable for large scale applications but it is applicable only in certain locations of area. Hydrogen is an attractive energy storage since it is one of the cleanest, lightest, and most efficient fuels, but it has a slow power response time. The disadvantage of the slow dynamics can be compensated through a implementing a suitable power management tool. Proper sizing of each component in a hybrid energy system is a key factor for its techno economic feasibility [9–11]. Unit sizing and technology selection can be based on meeting requirements such as using the available generation technology and not exceeding the equipment power rating, or on satisfying constraints and achieving multiple objectives such as minimizing environmental impact, installation , maintenance, investment and operating costs, payback periods on, with a maximized reliability. The optimization problem can sometimes have at variance goal and thus be complex. A completed survey of studies that addressed the complexities involved in the design of hybrid RE power generation technologies has been reported [12].

Significant research effort has been devoted to the modeling and control of individual process components as well as integrated RE systems. Most of the studies that have deal with hybrid energy systems have been performed in the simulation mode [5], [11], [13–17], with only a few dealing with real-time application [18]–[21] due to the high capital cost associated with design and implementation. The optimal combination of hydrogen storage with RE sources and the power management of such systems have also received significant attention [8]–[10], [18], [22–25].The importance of a control approach for the optimal operation of the photovoltaic (PV)/hydrogen/battery systems has been shown previously [23]. The output from the various generation sources of a hybrid energy system need to be corresponding and controlled to realize its full advantage. as a result, development of suitable power management that ensures meeting the customer load demand in the face of the irregular nature of RE sources is an important part of ensuring the system's reliability and achieving operational efficiency [26].

Here, I can describe the full model for the wind/PV/electrolyzer/fuel cell system and power management tool that utilizes decentralized adaptive model predictive control (MPC) at the local control level and decision-based control at the supervisory level. In this paper, power generated from wind and PV is stored in the form of hydrogen. Maximum power point tracking (MPPT) on the PV system and the pitch angle and power controllers on the wind turbine make certain optimal power generation by the RE sources. The supervisory controller computes the power references for the fuel cell and electrolyzer subsystems at each sampling time. The power references are sent to the local decentralized MPC system, which brings the fuel cell and electrolyzer subsystems to the desired power reference values while minimizing a suitable cost function. The modal proposed control design is evaluated through simulations.

II. PROCESS MODEL

Dynamic, first-principles models of the individual units along with their system combination are described in the following subsections. It is assumed that the electrochemical reactions in the electrolyses and fuel cell are instantaneous.

 While the model does not include phenomenon with a very slow response (i.e., catalyst and membrane degradation in the fuel cell and electrolyses), it captures the essential dynamics of the system and allows the achievement and evaluation of the proposed control approach.

A. Wind Energy Conversion System

 It is consists of a turbine to capture the kinetic energy in the wind, a drive train to speed set up the rotational speed of the shaft, than, a generator to convert the mechanical energy into electrical energy (Fig. 1). In this paper, a variable-speed wind turbine with the capability of continuous adjustment (i.e acceleration or deceleration) of the rotational speed " " of the wind turbine to the wind speed "*v*" is used. The classification of variable-speed wind turbines is according to generator used, among them, WECS equipped with doubly fed inductance generators (DFIGs) are the most common type used In this, pitch control with an efficient transmission of the power to the grid through active and reactive power control has made because they are very attractive due to the increasing issue of the wind power impact on the electrical network system. In these above types of generators, the stator out put terminals of the generators is directly connected to the grid and the rotor is handled by converters [28].

In this model consists of three main parts: wind turbine rotor, drive train, and generator. The wind turbine rotor converts the kinetic energy of the wind into mechanical energy by producing torque.
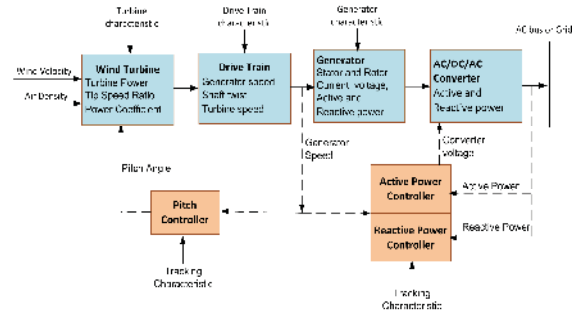
Fig. 1. Wind energy conversion block diagram.

Since the kinetic energy of wind contained a wind form, its magnitude depends on the air density and wind velocity. The wind power obtained by the turbine rotor is given by [15], [25], and [29]

$$P_w = \frac{1}{2}\rho A v^3 c_p(\lambda, \beta) \qquad (1)$$

Where **Pw** is the power extracted from the wind, is the air density, **A** is the swept area by the wind, and **cp** is the power coefficient which is a function of the tip speed ratio and the pitch angle of the rotor blades . The tip speed ratio is described as [29].

$$\lambda = \frac{\omega_m R}{v} \qquad (2)$$

Where $_m$ is the rotational speed and **R** is the radius of the wind turbine rotor. The drive train transfers the power from the turbine rotor to the generator.

It includes the input rotating shaft connected to the gear box and the output shaft connecting the drive train to the generator. The main model equations for the drive train are as follows [29-30]:

$$\frac{d\omega_m}{dt} = \frac{1}{2H_m}\left(T_m - K\theta_{mg} - D_m\omega_m\right) \qquad (3)$$

$$\frac{d\omega_g}{dt} = \frac{1}{2H_g}\left(K\theta_{mg} - T_e - D_g\omega_g\right) \qquad (4)$$

$$\frac{d\theta_{mg}}{dt} = \omega_0\left(\omega_m - \omega_g\right) \qquad (5)$$

Where **Tm** is the accelerating torque, **Te** is the decelerating torque, K is the effective shaft stiffness, $_{mg}$ is the twist in the shaft system, $_g$ is the generator speed, $_0$ is speed constant of the system, D_m $_m$ is the damping torque in the wind turbine, and D_g $_g$ is the damping torque in the generator. It is assumed that the shaft stiffness is constant. A model that is commonly used for the synchronous generator is the Park model [31]. The stator is directly connected to the grid and the stator voltage (v_s) is imposed by the grid. The rotor voltage (v_r) is controlled by a converter and this voltage is used to control the captured power from the wind generator [29]. A set of converters on the rotor side provides an opportunity to manipulate the rotor side voltage and consequently the captured power. The main generator model equations are as follows [31]:

$$\vec{v}_s = R_s\vec{i}_s + \frac{d\vec{\psi}_s}{dt} \qquad (6)$$

$$\vec{v}_r = R_r\vec{i}_r + \frac{d\vec{\psi}_r}{dt} - j\omega_r\vec{\psi}_r. \qquad (7)$$
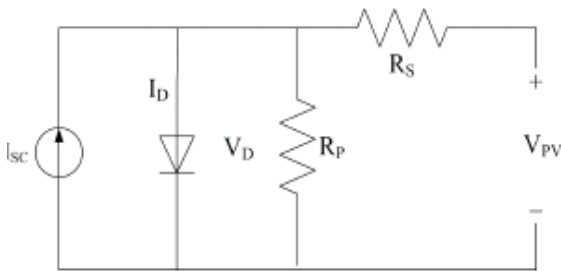
Fig. 2. Equivalent circuit model for a PV cell.

The stator and rotor fluxes are given by

$$\vec{\psi}_s = L_s\vec{i}_s + L_m\vec{i}_r \qquad (8)$$

$$\vec{\psi}_r = L_r\vec{i}_r + L_m\vec{i}_s \qquad (9)$$

Where $\vec{i}_s$ is the current space vector, v_s and v_r are the rotor and stator voltage space vectors, respectively, Lm is the Magnetizing inductance, Ls and Lr are the rotor and inductor self-inductances, respectively, Rs and Rr are the rotor and stator resistance, respectively, and $_s$ and $_r$ are the rotor and stator flux space vectors, respectively.

B. Solar Energy Conversion System

The solar energy conversion system orthe physical of PV cell is very similar to that of the classical diode with a PN junction formed by semiconductor material. When the junction absorbs light, the energy of absorbed photon is transferred to the electron-proton system of the material, creating charge carriers that are separated at the junction. The charge carriers in the junction region create a potential gradient, get accelerated under the electric field, and circulate as current through an external circuit. The solar cell is the basic building of the PV power which solar energy is converted directly into electrical energy. A solar cell is usually represented by an electrical equivalent one P- N junction diode model as shown in Fig. 2. The model contains a short-circuit current Isc, a diode, and a series resistance R_S and the resistance R_P inside each cell and in the connection between the cells. The correlation between the output PV voltage and the current of a PV cell or a module can be expressed as [32].

$$I_{pv} = I_{sc} - I_D - \frac{V_D}{R_P} \qquad (10)$$

$$V_{pv} = V_D - R_S I_{pv} \qquad (11)$$

$$I_D = I_0\left(e^{(V_D/V_T)} - 1\right) \qquad (12)$$

Where I_0 is the saturation current, V_D is the diode voltage, I_D is the diode current, and V_T is the diode voltage. Standard PV characteristics are needed to solve the model, including the short-circuit current Isc, the open-circuit voltage Voc, the rated current I_R, and the voltage V_R at the maximum power point (MPP) under standard test conditions (25 °C). The effect of temperature on the PV panel is not considered. Cells are normally grouped into modules, which are then connected in arrays with MP parallel branches, each with MS modules in series. Under the assumption that the modules are identical and are all exposed to the same ambient irradiation, the solar cell arrays

$$I_a = M_P I_{pv} \qquad (13)$$

$$V_a = M_S V_{pv}. \qquad (14)$$
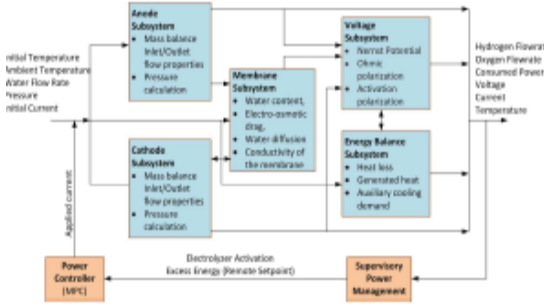
Fig. 3. Electrolyzer modeling block diagram.

C. Hydrogen Generation (PEM Electrolyzer) System

The electrolysis of water using cells with a polymer electrolyte membrane (PEM) is a very efficient method of producing hydrogen. PEM electrolyzers are very simple and compactable and have conventional higher current density capacity than conventional alkaline water electrolyzers. The reactions are take place at anode and cathode of a PEM electrolyzer are described below

$$\text{Anode Reaction}: H_2O \rightarrow 2H^+ + \frac{1}{2}O_2 + 2e \quad (15)$$

$$\text{Cathode Reaction}: 2H^+ + 2e \rightarrow H_2. \quad (16)$$
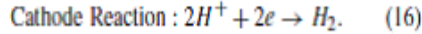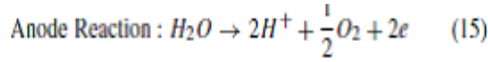
At anode side, the supplied water is decomposed into oxygen gas, hydrogen protons, and electrons. In this reaction, hydrogen protons are transported through the proton conductive membrane to the cathode side. And the same time, the electrons exit the PEM electrolyzer cell through the external circuit, in the case supplies the driving force (i.e., cell potential) for the reaction, at cathode side, the hydrogen protons and the external circuit electrons recombine to form hydrogen gas. The model for a PEM electrolyzer is composed of four parts: such as anode, cathode, membrane, and voltage ancillary (Fig. 3). In the anode system, calculates oxygen and water flows and their partial pressures. Cathode system calculates hydrogen and water partial pressures and their flows. And membrane system Determine the water content, drag, water diffusion, and the conductivity of a membrane. The voltage auxiliary calculates the electrolyzer's voltage by the Nernst equation, ohmic polarization, and activation polarization. The material balance equations for the anode side are given by

$$\text{Anode}: \begin{cases} \frac{dN_{O_2}}{dt} = N_{O_2}^{in} - N_{O_2}^{out} + N_{O_2}^{gen} \\ \frac{dN_{H_2O}}{dt} = N_{H_2O}^{in} - N_{H_2O}^{out} - N_{H_2O}^{mem}. \end{cases} \quad (17)$$

The number of moles of water N_{H2O} and oxygen N_{O2}, the electrolyzer temperature, and the water and oxygen partial pressures pH_2O and p_{O2} are used to calculate the anode total pressure

P Anode $= pH2O + pO2$ and the oxygen mole fraction y_{O2} inside the anode channel using the ideal gas law and thermodynamic properties. Electrochemistry principles are used to calculate the rates of oxygen generation N_{gen} ^{O2} during the water splitting reaction. The rate of generated oxygen is obtained from Faraday's law as

$$N_{O_2}^{gen} = \frac{n_{ele} I_{ele} \eta_F}{n_{st} F} \quad (18)$$

Where **nele** is the number of electrolyzer cells, **Iele** is the electrolyzer applied current, **nst** is the reaction stoichiometry coefficient, F is the Faraday efficiency, and F is the Faraday constant. Similar to the anode ancillary, the cathode molar flows of water and hydrogen are obtained by calculating the partial pressures p_{H2O} and p_{H2}, respectively, cathode total pressure p_C, and the hydrogen mole fraction

$$\text{Cathode}: \begin{cases} \frac{dN_{H_2}}{dt} = N_{H_2}^{in} - N_{H_2}^{out} + N_{H_2}^{gen} \\ \frac{dN_{H_2O}}{dt} = N_{H_2O}^{in} - N_{H_2O}^{out} + N_{H_2O}^{mem}. \end{cases} \quad (19)$$

The rate of hydrogen generated in the water-splitting reaction, $N_{H_2}^{gen}$ is a function of the stack current

$$N_{H_2}^{gen} = \frac{n_{ele} I_{ele} \eta_F}{n_{st} F}. \quad (20)$$

The water transport through the membrane is achieved by electro-osmotic drag and diffusion phenomena. Note that the membrane molar rate is needed to calculate the molar rates in the anode and cathode ancillaries [(17) and (19)]. The amount of water transported is dependent on the electro osmotic drag coefficient **nd**, which is defined as the number of water molecules carried by each proton. Water diffusion through the membrane is calculated by Fick's law, and the combination of these two phenomena is shown in the following equation:

$$N_{H_2O}^{mem} = M_{H_2O} A_{ele} \left(n_d \frac{\bar{I}_{ele}}{F} + D_w \frac{c_{w,c} - c_{w,a}}{t_m} \right) \quad (21)$$

where M_{H2O} is molecular weight of water, A is the area of the electrolyzer cell, **lele** is the current density, Dw is the water diffusion coefficient, $c_{w,c}$ and $c_{w,a}$ are the water concentration at the cathode and anode surface, respectively, and t_m is the thickness of the membrane.

The electro-osmotic drag and diffusion coefficient vary with the water content in the membrane, i.e., **m,** and empirical relationships describing these correlations. The total electrolyzer voltage can be represented as

$$V_{ele} = E_{ele} + V_{ele}^{act} + V_{ele}^{ohm} \tag{22}$$

where *E*ele is the open-circuit voltage, V_{ele}^{act} is the activation polarization, and V_{ele}^{ohm} is the ohmic polarization. The open circuit voltage (*E*ele), defined by the Nernst equation and the activation and ohmic over potentials are modeled.

$$\begin{cases} E_{ele} = \frac{1}{2F}\left(\Delta G_{ele} + RT_{ele}\left[ln\left(\frac{p_{H_2}^{ele}\sqrt{p_{O_2}^{ele}}}{a_{H_2O}^{ele}}\right)\right]\right) \\ V_{ele}^{act} = \frac{RT_{ele}}{2\beta F}ln\left(\frac{\bar{I}_{ele}}{\bar{I}_{ele0}}\right) \\ V_{ele}^{ohm} = \bar{I}_{ele}R_{ele}^{ohm} \end{cases} \tag{23}$$

where *R* is the universal gas constant, *G*ele is the Gibbs free energy of formation, *T*ele is the absolute temperature, $a_{H_2O}^{ele}$ is the water activity between the anode and the electrolyte
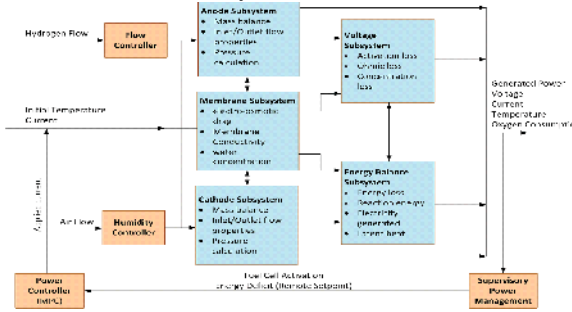
Fig. 4. Fuel cell modeling block diagram.

$p_{H_2}^{ele}$ and $p_{O_2}^{ele}$ are the partial pressures of hydrogen, andoxygen, respectively. The activation polarization is a function

of the current density $\bar{I}_{ele}$, the exchange current density $\bar{I}_{ele0}$,

and the charge transfer coefficient . The ohmic polarization is a function of the membrane resistance R_{ele}^{ohm}, which can be calculated by using the membrane conductivity and its thickness. Assuming a lumped thermal capacitance model, the overall thermal energy balance can be expressed as [22] and [25].

$$C_{ele}\frac{dT_{ele}}{dt} = \dot{Q}_{gen} - \dot{Q}_{loss} - \dot{Q}_{cool} \tag{24}$$

where *C*ele is the overall heat capacity of the electrolyzer, ˙*Q*gen is the heat power generated inside the electrolyzer stack, ˙*Q* loss is the heat power loss, and ˙*Q* cool is the heat power loss due to cooling. Each term in the thermal energy balance equation is calculated as follows:

$$\begin{cases} \dot{Q}_{gen} = n_{ele}I_{ele}(V_{ele} - V_{th}) \\ \dot{Q}_{loss} = \frac{T_{ele}-T_0}{R_{ele}^{th}} \\ \dot{Q}_{cool} = C_{ele}^{m}(T_m^{out} - T_m^{in}) \end{cases} \tag{25}$$

where *V*th is the thermal voltage, *T*0 is the ambient temperature, R_{ele}^{th} is the thermal resistance, C_{ele}^{m} is the cool ingmedium overall heat capacity, and *Tm* is the cooling medium temperature.

D. Hydrogen Consumption (Fuel Cell) System
The reverse equivalent of a PEM electrolyzer is a PEM fuel cell, which is thus modeled similar to the PEM electrolyzer described in the previous section. Chemical energy of the hydrogen fuel is converted into electricity through a chemical reaction with oxygen. The byproducts of this reaction are water and heat. The dynamic fuel cell model used here was developed and it is divided into four main ancillaries: the anode, the cathode, the membrane, and the voltage (Fig. 4). The mole balance equations for oxygen, nitrogen, hydrogen, and water mass on the anode and cathode side of the PEM fuel cell can be written as follows:

$$\text{Anode}: \begin{cases} \frac{dN_{H_2}}{dt} = N_{H_2}^{in} - N_{H_2}^{out} + N_{H_2}^{reac} \\ \frac{dN_{H_2O}}{dt} = N_{H_2O}^{in} - N_{H_2O}^{out} - N_{H_2O}^{mem} \end{cases} \tag{26}$$

$$\text{Cathode}: \begin{cases} \frac{dN_{O_2}}{dt} = N_{O_2}^{in} - N_{O_2}^{out} + N_{O_2}^{reac} \\ \frac{dN_{H_2O}}{dt} = N_{H_2O}^{in} - N_{H_2O}^{out} + N_{H_2O}^{gen} + N_{H_2O}^{mem} \\ \frac{dN_{N_2}}{dt} = N_{N_2}^{in} - N_{N_2}^{out}. \end{cases} \tag{27}$$

The molar rate of water inside the cathode, *N*H2O, depends on the summation of vapor flows, because it is assumed that the liquid water does not leave the stack and evaporates into the cathode gas if cathode humidity drops below 100%. Water is in vapor form until the relative humidity of the gas exceeds saturation (100%), at which point the vapor condenses into liquid water. Similar to the electrolyzer, the ideal gas law, thermodynamic properties, and electrochemistry principles can be used to calculate the components' partial pressures, total pressure at the anode and cathode, moles of reacted hydrogen and oxygen, as well as the generated water. The fuel cell voltage is calculated based on voltage drops associated with all the losses as follows. The fuel cell voltage is calculated based on voltage drops associated with all the losses as follows:

$$V_{fc} = E_{fc} - V_{fc}^{act} - V_{fc}^{ohm} - V_{fc}^{conc} \qquad (28)$$

where V_{fc} is the fuel cell voltage, E_{fc} is the open-circuit voltage, V_{fc}^{act} is the activation polarization, V_{fc}^{ohm} is the ohmic polarization, and V_{fc}^{conc} is the concentration over potential. The open-circuit voltage and ohmic polarization are calculated as in 23. The activation and concentration over potentials are obtained by the following equations:

$$\begin{cases} V_{fc}^{act} = V_0^{act} + c_{act,1}\left(1 - e^{c_{act,2}\bar{I}_{fc}}\right) \\ V_{fc}^{conc} = \bar{I}_{fc}\left(c_{conc,1}\frac{\bar{I}_{fc}}{I_{fc}^{max}}\right)^{c_{conc,2}} \end{cases} \qquad (29)$$

where V_n^{act} is the fuel cell current density, V_0^{act} is the voltage drop at zero current density, and a $c$act and $c$conc and $\bar{I}_{fc}^{max}$ are constants that depend on the temperature and reactant partial pressure and are obtained empirically. The heat generated by the fuel cell chemical reaction can be written as

$$C_{fc}\frac{dT_{fc}}{dt} = \dot{Q}_{gen} - \dot{Q}_{elec} - \dot{Q}_{s.+l.} - \dot{Q}_{loss} \qquad (30)$$

where $\dot{Q}$gen is the heat generated from chemical reaction, Qelec is the generated electrical energy, Qs.+l. is the absorbed latent and sensible heat, and Q loss is the heat loss. These terms are given by the following relations:

$$\begin{cases} \dot{Q}_{gen} = N_{H_2}^{reac} \Delta H_{fc}^{reac} \\ \dot{Q}_{elec} = V_{fc} I_{fc} \\ \dot{Q}_{s.+l.} = \sum_{i=H_2,O_2,H_2O} C_i \\ \qquad \times \left(N_i^{out}T_{fc} - N_i^{in}T_{in}\right) + N_{H_2O}^{gen}\Delta H_v \\ \dot{Q}_{loss} = h_{fc}A_{fc}\left(T_{fc} - T_{amb}\right) \end{cases} \qquad (31)$$

where

ΔH_{fc}^{reac} is the enthalpy of reaction, C_i is the specific heat capacity, H_v is the heat of evaporation, $h$fc is the fuel cell heat transfer coefficient, Afc is the fuel cell surface area, and T amb is the ambient temperature. The detailed model for all the fuel cell ancillaries can be found in [25].

E. Hydrogen Storage System
Hydrogen storage consists of a compressor and a hydrogen tank. The required compression work can be estimated as follows [25].

$$P_{comp} = N_{H_2}^{out}|ele\frac{Zn_cRI_{in}}{\eta_c(n-1)} \times \left(\left(\frac{P_{out}}{\sqrt{P_{in}P_{out}}}\right)^{\frac{n_c-1}{n_c}} - 1\right) \qquad (32)$$

where P_{comp} is the compressors consumed power, Tin is the hydrogen temperature from the electolyzer (assumed to be equal to T_{ele}), and $_c$ is the compressor efficiency. The hydrogen mole balance in the tank is obtained as

$$\frac{dN_{H_2}}{dt}\bigg|_{tank} = \frac{N_{H_2}^{in}}{dt}\bigg|_{fc} - \frac{N_{H_2}^{out}}{dt}\bigg|_{ele}. \qquad (33)$$

Accumulated hydrogen in the tank calculated by 33 is used to estimate the hydrogen pressure in the tank under the assumption that the tank temperature T tank is constant, using the Beattie–Bridgeman equation [25].

$$P_{tank} = \frac{N_{H_2}^{tank\,2}RT_{tank}}{V_{tank}^2}\left(1 - \frac{a_1 N_{H_2}^{tank}}{V_{tank}T_{tank}^3}\right) \\ \times \left[\frac{V_{tank}}{N_{H_2}^{tank}} + a_2\left(1 - \frac{a_3 N_{H_2}^{tank}}{V_{tank}}\right)\right] \\ - \frac{a_4\left(1 - \frac{a_5 N_{H_2}^{tank}}{V_{tank}}\right)N_{H_2}^{tank\,2}}{V_{tank}^2} \qquad (34)$$

where P tank is the tank pressure, V tank is the tank volume, and a_1–a_5 are empirical parameters [25].

III. CONTROL ARCHITECTURE

A Different types control scheme has been reported as a more practical and efficient chain of command for controlling hybrid energy systems. In this control structure for the system studied, it has consists of two layers, namely, supervisory controller and low-level local controllers. The supervisory control system monitors and controls the power flow from the Solar/wind sources to the storage components and power consumption centers. It also determine the operating trajectories for the fuel cell and electrolyzer subsystems. The local controller system is responsible for regulating each process component to improve efficiency and its performance. All process subsystems and their controllers are connected to the supervisory controller. This control scheme goal to fulfill the following objectives.
1) Optimally using the energy resources.
2) Meeting the load demand.
3) Operating the system efficiently.
In the following subsections, these two control system are described in detail.

A. Supervisory Power Control

The hybrid energy system consists of the power generation (wind, PV, and fuel cell) and the power consumption components (electrolyzer, auxillary equipment, and the main load demand). Power flow in the hybrid system is shown in Fig. 5. The net power (Pnet), which is the difference between the generation sources and the load demand, is calculated as

$$P_{net} = \left(P_{wind} + P_{pv} \right) - \left(P_{load} + P_{ae} \right) \tag{35}$$

Where P_{wind} and P_{pv} are the power generated by the wind and solar energy conversion systems, respectively, P_{load} is the load demand, and P_{ae} is the
power consumed by auxiliary equipment in the system. The generated power from the renewable sources can be either used directly to meet the load demand or transferred to the hydrogen production process. Because of the alternating nature of RE as well as the dynamic load demand, P_{net} can have a positive, zero, or negative value at any instant. In the case of $P_{net} = 0$, there is sufficient power generated from the renewable sources to meet the load and auxiliary equipment demand with neither excess nor deficit of energy. The electrolyzer and fuel cell activation and deactivation are based on the Pnet value which is calculated in each sampling interval. When there is excess power generated ($P_{net} > 0$), the electrolyzer is activated. On the other hand, when there is adeficit in power generation ($P_{net} < 0$), the fuel cell stack is activated to consume previously stored hydrogen and convert it to electricity. The fuel cell activation will occur only if there is a sufficient supply of hydrogen in the storage tank. Otherwise, the hybrid system enters a "hydrogen starvation" mode. This can occur as a consequence of either extreme operational conditions, such as low availability of renewable sources and very high load demand, or inappropriate unit sizing. The power management logic is shown below

$$
\begin{cases}
\text{If } (P_{net} > 0) \\
\quad \rightarrow \left(\zeta_{ele} = 1, \quad \zeta_{fc} = 0, \quad \zeta_{comp} = 1 \right) \\
\text{If } (P_{net} > 0 \ \ \& \ \ P_{tank} \geq P_{tank}^{ub}) \\
\quad \rightarrow \left(\zeta_{ele} = 0, \quad \zeta_{fc} = 0, \quad \zeta_{comp} = 0 \right) \\
\text{If } (P_{net} < 0 \ \ \& \ \ P_{tank} \geq P_{tank}^{lb}) \\
\quad \rightarrow \left(\zeta_{ele} = 0, \quad \zeta_{fc} = 1, \quad \zeta_{comp} = 0 \right) \\
\text{If } (P_{net} < 0 \ \ \& \ \ P_{tank} < P_{tank}^{lb}) \\
\quad \rightarrow \left(\zeta_{ele} = 0, \quad \zeta_{fc} = 0, \quad \zeta_{comp} = 0 \right) \\
\text{If } (P_{net} = 0) \\
\quad \rightarrow \left(\zeta_{ele} = 0, \quad \zeta_{fc} = 0, \quad \zeta_{comp} = 0 \right).
\end{cases} \tag{36}
$$

In the above P_{tank}^{lb} and P_{tank}^{ub}, are the low hydrogen pressure tanks lower and higher limits, respectively, and ζ_{ele}, ζ_{fc}, and ζ_{comp} are the operational modes (ON/OFF) for the electrolyzer, fuel cell, and compressor, respectively. According to (36), the electrolyzer becomes activated as soon as there is positive P_{net}. However, if the excess power is less than the electrolyzers rated power, the generated power will be completely used to keep the electrolyzer running while not satisfying the load demand. Equation (36) can be modified as follows to prevent this problem
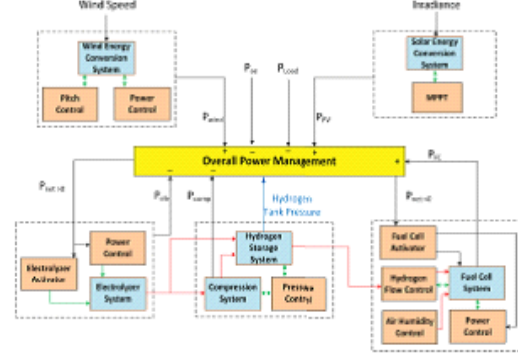
Fig. 5. Supervisory power management block diagram.

$$
\begin{cases}
\text{If } \left(P_{net} > P_{ele}^{rated} \right) \\
\quad \rightarrow \left(\zeta_{ele} = 1, \quad \zeta_{fc} = 0, \quad \zeta_{comp} = 1 \right)
\end{cases} \tag{37}
$$

where P_{ele}^{rated} is the electrolyzers rated power

B. Local Controllers

Each component in the studied hybrid energy system has its own local controller which enforces optimal operation of the corresponding unit based on the available information with respect to power generated from the WECS and PV, and power demand.

Wind System Controllers: The wind turbine power output varies with the wind speed, and this dependency is represented by a wind turbine characteristic curve. The characteristic curve has three distinct zones according to the corresponding wind speeds: cut-in, rated, and cut-out. Below the cut-in wind speed and above the cut-out wind speed, the output power is zero. When the wind velocity is between the cut-in and rated wind speeds, the local controller is responsible to extract the maximum power according to the wind turbine characteristic curve. This is achieved by controlling the active and reactive power of the rotor. The control scheme consists of two series
of two proportional integral (PI) controllers. The actual turbine speed (ω_m) and wind turbine characteristic are used to estimate the maximum possible power as a reference. The active and reactive power is compared to its reference, and the offset for both are sent to two stage controllers to adjust the current and voltage of the rotor converter side in order to obtain the maximum possible power.

The switching dynamics, the power losses in the converter, and delays caused by the intermediate dc converter are assumed to be negligible. Between the rated and cut-out wind speeds, the DFIG wind turbine activates a blade pitch angle controller to reduce the power coefficient and, consequently, the extracted power from the wind. This controller prevents high generator speed, and hence prevents mechanical damage of the turbine. The control action is based on comparing the generator speed to its reference and sending the error signal to PID controller, which estimates the reference value for the pitch angle. The offset between reference and actual pitch angle is minimized by a second P controller.

2) Solar System Controllers: Despite all improvements, PV modules still have a relatively low conversion efficiency. The voltage–current–Power
(V–I–P) characteristic curves for a PV array specifies a unique operating point at which the maximum possible power is delivered. The MPPT algorithm is used for extracting the maximum available power from the PV module under certain voltage and current conditions. There are several MPPT techniques reported in the literature. The perturbation and observation method (P&O) is one of the most common and effective ways of power tracking for PV arrays. In this paper, the current perturbation and observation method (CP&O) is applied. The MPP tracker operates by periodically incrementing or decrementing the solar array current (I_{pv}). If a given perturbation leads to an increase (decrease) of the output power of the PV (P_{pv}), then the subsequent perturbation is generated in the same (opposite) direction. The perturbation magnitude was set to 0.02 A.

3) Model Predictive Control of Electrolyzer and Fuel Cell:
Implementation of power control over the electrolyzer and the fuel cell can improve their efficiency and consequently the hydrogen generation and storage. The constraints and dynamics of the electrolyzer and fuel cell are decoupled as they operate in a sequential mode; i.e., when the fuel cell is ON (OFF), the electrolyzer is OFF (ON). A decentralized MPC scheme was employed to regulate the power of the electrolyzer and fuel cell. A key advantage of MPC is its ability to deal with constraints in a systematic and straightforward manner. This is of particular importance for the PEM electrolyzer and fuel cell operation, where abrupt changes in the current load produce more uneven water/current distribution and promote degradation of the membrane, which in turn decreases the overall efficiency and the working life of these units.

A decentralized approach is the most appropriate one because of the limited exchange of information between the subsystems. Moreover, a decentralized implementation of MPC has the advantage of reducing the optimization problem into a number of smaller and easily tractable ones. Each controller determines the constraint-admissible and optimum value of the current that can be applied on the electrolyzer/fuel cell at each sampling time. For control design purposes, the nonlinear models of the electrolyzer and fuel cell were linearized and discretized using the first-order hold conversion method. The resulting state space model has the form

$$\begin{cases} x(k+1) = Ax(k) + Bu(k) + Dd(k) \\ y(k) = Cx(k) \end{cases} \quad (38)$$

where k is the sampling time, and A, B, D, and C are matrices of appropriate dimensions. x, u, d, and y are the modelstates, manipulated variables, disturbances, and model outputs, respectively. The electrolyzer state space model variables are

$$\begin{cases} x_{ele} = \left[\delta N_{O_2}^a, \delta N_{H_2O}^a, \delta N_{H_2}^c, \delta N_{H_2O}^c\right]^T \\ y_{ele} = \left[\delta P_{ele}, \delta V_{ele}, \delta N_{H_2}, \delta p_{H_2}\right]^T \\ u_{ele} = [\delta I_{ele}], \\ d_{ele} = \left[\delta T_{ele}^a\right] \end{cases} \quad (39)$$

where the operator indicates the deviation from the operating point, and the *a* and *c* superscripts stand for anode and cathode, respectively. *P*ele is the controlled variable, while the rest of the outputs are measured ones. The fuel cell state space model variables are

$$\begin{cases} x_{fc} = \left[\delta p_{fc}, \delta N_{H_2}^a, \delta N_{H_2O}^a \delta N_{N_2}^c, \delta N_{O_2}^c\right]^T \\ y_{fc} = [\delta P_{fc}, \delta V_{fc}]^T \\ u_{fc} = [\delta I_{fc}] \\ d_{fc} = \left[\delta T_{fc}^c\right] \end{cases} \quad (40)$$

where P_{fc} is the fuel cell generated power chosen as the controlled variable, T_{fc}^c is the input air temperature, and V_{fc} is the fuel cell voltage (the measured output). For both systems, the control objective is imposed at any instant by the P_{net} value from the power management controller. The model predictive controller is designed to minimize the following finite horizon control and performance index:

$$\min_u J(x(t), u(t), t) = \begin{cases} \sum_{k=1}^{H_p} W_y \left[y(k) - y(k)_{ref}\right]^2 \\ + \sum_{k=1}^{H_c} W_u \left[u(k) - u(k)_{ref}\right]^2 \\ + \sum_{k=1}^{H_c} W_u \left[\Delta u(k|k+1)\right]^2 \end{cases} \quad (41)$$

$$\text{subject to} : \begin{cases} y(k)_{lb} < y(k) < y(k)_{up} \\ u(k)_{lb} < u(k) < u(k)_{up} \\ \Delta u(k)_{lb} < \Delta u(k) < \Delta u(k)_{up} \end{cases} \quad (42)$$

where *Wy* and *Wu* are input and output weight factors for each variable, and H_P and H_C are the prediction and control horizons, respectively. The objective function was subjected to a set of constraints, consisting of the fuel cell and electrolyzer output power upper and lower limits *(y_{ub}, y_{lb})*, current upper and lower limits *(u_{ub}, u_{lb})*, and the rate of change in the electrolyzer and fuel cell current *(u)*. The output power upper and lower limits *(y_{ub}, y_{lb})* are defined by the fuel cell and electrolyzer power operating range. Two sets of operating conditions, which correspond to 10% and 90% of the rated power for the fuel cell and electrolyzer, were used for model linearization. The resulting linear models are provided in Supporting Information. Based on these linearized models, two MPC controllers were designed for each unit. In each control period, a suitable controller is chosen to enforce the remote power set point calculated by the supervisory controller. If the signal value was <50% of the rated power, the low operating range controller was selected. Otherwise, the high operating range controller was chosen.

Table 1: Summarized System Component Sizing Used In Simulation.

Wind system	Rated power	4 kW
	Cut-in speed	3 m/s
	Cut-out speed	12 m/s
	Rated speed	7 m/s
PV system	Rated power	120 W/panel
	Total rated power	2.4 kW
	PV array	20 ×2
	Temperature	25 °C
Electrolyzer	Rated power	2.8 kW
	H_2 Flow rate	8 slpm
	Output pressure	14 atm
H_2 Storage	Tank volume	50 m^3
	Tank pressure	150–200 atm
	Compressor pressure	200 atm
Fuel cell	Rated power	1.9 kW
	H_2 Flow rate	15 slpm
Load	Power	1–2 kW

This strategy is advantageous, as it minimizes the model mismatch by having multiple models while significantly simplifying its implementation, which is of particular importance for real-time studies. Aside from the power control, the fuel cell has two additional PI controllers which minimize the pressure difference between the cathode and anode by manipulating the hydrogenflow and keep the desired air humidity by injecting the appropriate amount of water vapor into the air stream entering the cathode side, respectively.

IV. RESULTS AND DISCUSSION

The proposed hybrid stand-alone system model consisting of the previously described components was implemented using the MATLAB and Simulink software. Model testing was performed under various conditions using historical wind data, irradiance, ambient temperature, as well as dynamic load demand data. The sizing of the process components in the existing stand-alone system is shown in Table 1. The sizing of the various process components was performed according to the electricity energy balance for small loads typical of residential demand. This load demand is intermittent in nature, and it was assumed that its minimum, maximum, and average alues are 0.5, 1.9, and 1 kW, respectively. The sizing was performed according to the net power, which is estimated based on the difference of the power generated by wind and PV and the power demand at all times. Assuming a capacity factor (combination of the overall unit efficiency and the effect of geographical location) of 15% and 10% for the wind turbine and PV array, respectively, 4-kWrated wind power and 2.4-kWPV rated power were estimated.

The fuel cell needs to supply the maximum load demand when there is no sufficient power generated by the PV and wind. Therefore, the estimated size of the fuel cell stack is 1.9 kW. The electrolyzer capacity should be adequate to use the surplus power from the RE sources. The maximum excess power will occur when there is minimum load and maximum power from the RE sources, which corresponds to 6.4 kW of electrolyzer capacity. However, the situation when both wind and solar power reach their maximum points while the load demand is at its lowest is very unlikely, and thus a 2.8 kW capacity for the electrolyzer was used. The presented simulation results are based on the average weather data for a winter day in the Sarnia, Ontario region, and the load demand for the installed stand-alone system. Table 2 presents the PID tuning parameters for the various low-level controllers applied on the wind and fuel cell subsystems. In this table, *kc*, *i*, and *d* are the proportional, integral, and derivative constants, respectively. The wind and irradiance data along with the corresponding generated power is shown in Fig. 6(a) and (b). As was mentioned previously, between the cut-in and rated speeds (3 and 7 m/s) the WECS power control is regulating the generator converter to generate the maximum possible power by manipulating the turbine speed. Above the wind speed of 7 m/s, the pitch controller is maintaining the power at the rated wind turbine power, as is shown in 6(c). Fig. 7(a) shows the total generated power, the load demand, and their difference (*P*net).

The *P*net trend shown in Fig. 7(a) is used to activate or deactivate the hydrogen system components. Fig. 7(b) presents the electrolyzer and fuel cell status throughout the simulation period. When *P*net >*P*elethere is excess power available for hydrogen generation, which will result in the activation of the electrolyzer at its rated capacity. In the case of *P*net <0, the fuel cell is activated to supply the power deficit [see Fig. 7(b)]. As mentioned previously, the objective of the power management supervisory controller is not only to enable anddisable the hydrogen system components but also to send the remote set point to the fuel cell and electrolyzer via *P*net.
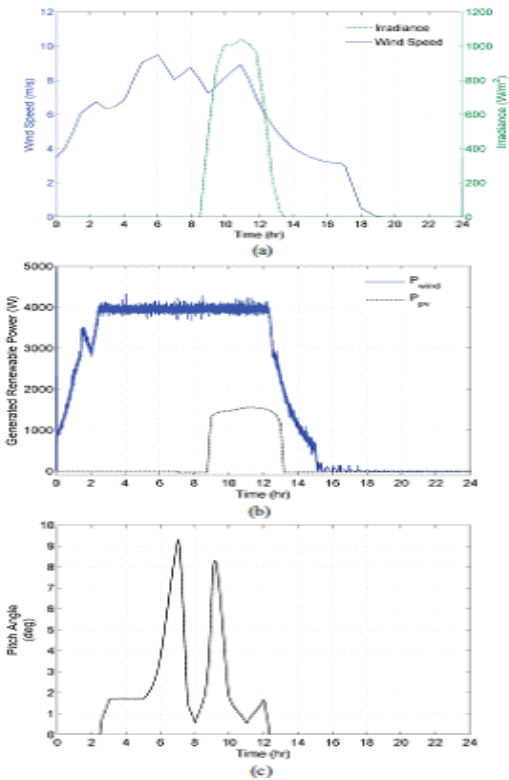
Fig. 6. RE conversion systems. (a) Wind speed and solar data. (b) Generated power. (c) Pitch angle controller output for wind turbine.

Table 2: Controller Tuning Parameters.

Wind pitch controller	Reference pitch estimator	PD controller: $k_c = 35$, $\tau_d = 0.2$
	Pitch angle controller	P controller: $k_c = 500$
Wind power controller	Rotor side current controller	PI controller: $k_c = 0.3$, $\tau_i = 0.037$
	Grid side current controller	PI controller: $k_c = 1$, $\tau_i = 0.01$
	Voltage controller	PI controller: $k_c = 0.02$, $\tau_i = 0.4$
Fuel cell controller	Hydrogen flow controller	PI controller: $k_c = 1.2$, $\tau_i = 0.01$
	Air humidity controller	P controller: $k_c = 1$
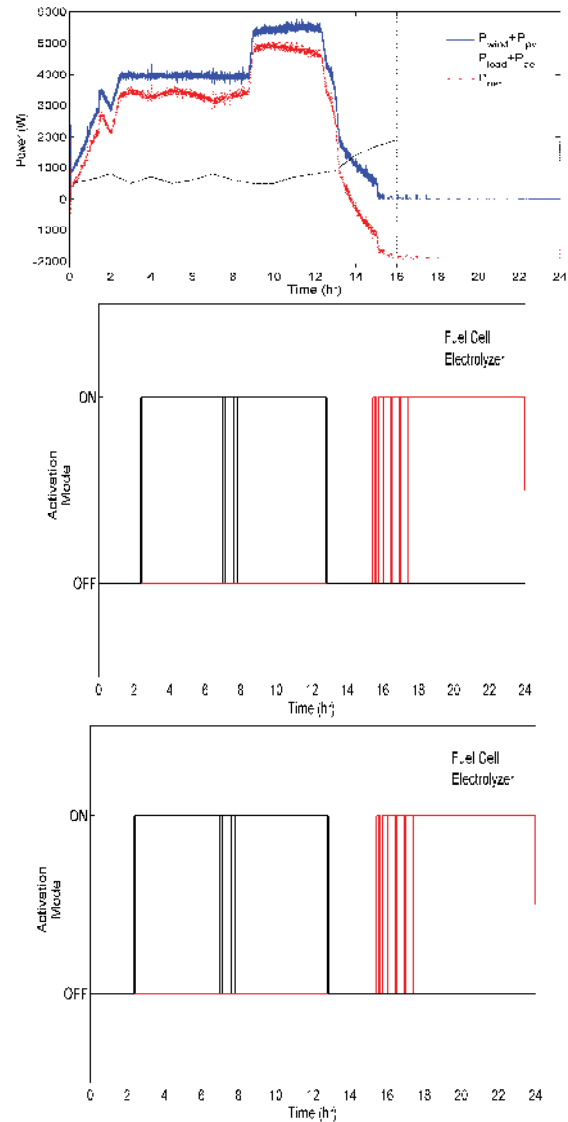
Fig. 7. Power balance and hydrogen system components activation. (a) Power trends including net power, total generated RE and load demand with auxiliary equipment consumption. (b) Electrolyzer and fuel cell activation/deactivation.

The model predictive controller was designed for the electrolyzer and fuel cell and then integrated with the nonlinear model of the plant. The length of the prediction horizon affects both the computational time and the performance of the system. The prediction horizon (*Wy*) and control horizon (*Wu*) was set to 15 and 8 intervals for the electrolyzer, and 10 and 4 intervals for the fuel cell. The operational range for the electrolyzer and fuel cell is 200–2800 and 100–1900W, respectively.
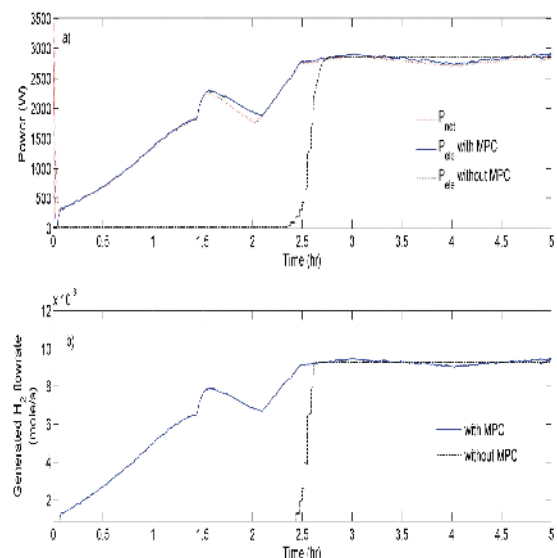
Fig. 8. Electrolyzer MPC. (a) Performance in terms of tracking net power. (b) Generated hydrogen.
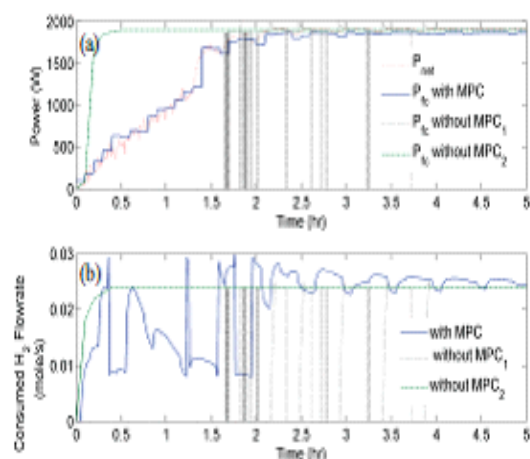
Fig. 9. Fuel cell MPC. (a) Performance in terms of power generated.(b) Consumed hydrogen.

A variable sampling time with maximum size of 1 s was used for data measurement. The remote set point for the MPC controllers was P net for the electrolyzer and $|P$net$|$ for the fuel cell. Figs. 8 and 9 show the performance of the MPC controllers implemented for the electrolyzer and fuel cell, respectively. The controllers show robust set-point tracking despite the variation in the set points. It is important to note that the hydrogen generation by the electrolyzer and its consumption by the fuel cell are significantly more efficient. Also, note that the ability to run the electrolyzer at lower capacity enablesits activation below its rated power (Prated ele). This in turn results in using the RE more efficiently and, consequently, in higher hydrogen generation. More importantly, MPC eliminates frequent turning on and off of the electrolyzer, which can decrease the lifespan of the unit

drastically. For the fuel cell, we demonstrate two criteria for the fuel cell activation without the power controller (Fig. 9). In the first criterion (without MPC1), P net <0 and $|P$net$|$ $>P$fc, which results in the more conservative hydrogen usage but also fails to meet the load demand. On the other hand, the second criterion (without MPC2), Pnet <0 and $|P$net $|$ $<P$fc, resulting in overgeneration of electricity as the fuel cell is always operated at its rated capacity with previously stored hydrogen depleting rapidly. The implementation of the MPC eliminates these problems and results in the successful demand tracking and adequate hydrogen usage, as shown in Fig. 9.

V. CONCLUSION

A full detailed model for a stand-alone hybrid energy system with wind turbine and solar energy conversion, electrolyzer, fuel cell, and hydrogen storage components was developed. A supervisory controller for proper power management and a set of local controllers for efficient hydrogen generation and consumption were implemented. A model predictive controller was designed for optimal operation of the electrolyzer and fuel cell. The controller performance showed significant improvement in the utilization of both components, and consequently better power management of the hybrid energy system could be achieved in comparison to the case when there was no model predictive controller. Future work will focus in Lambton College. We also plan to implement a dynamic optimization formulation at the supervisory level which would account for the weather and demand prediction to ensure smooth operation and minimization of the operational cost.

REFERENCES

[1] "Annual energy outlook 2011," U.S. Energy Inf. Administration, Washington,DC, USA, 2011.
[2] S. S. Dihrab and K. Sopian, "Electricity generation of hybrid PV/windsystems in Iraq," *Renew. Energy*, vol. **35**, no. 6, pp. 1303–1307, 2010.
[3] R. Dufo-López and J. L. Bernal-Agustín, "Multi-objective design of PV–wind–diesel–hydrogen–battery systems," *Renew. Energy*, vol. **33**, no. 12, pp. 2559–2572, Dec. 2008.
[4] M. A. Elhadidy and S. M. Shaahid, "Promoting applications of hybrid *(*Wind+Photovoltaic+Diesel+Battery*)* power systems in hot regions,"*Renew. Energy*, vol. **29**, no. 4, pp. 517–528, Apr. 2004.
[5] G. Giannakoudis, A. I. Papadopoulos, P. Seferlis, and S. Voutetakis,"Optimum design and operation under uncertainty of power systemsusing renewable energy sources and hydrogen storage," *Int. J. HydrogenEnergy*, vol. **35**, no. 3, pp. 872–891, 2010.
[6] M. Soroush and D. Chmielewski, "Process systems opportunities inpower generation, storage and distribution," *Comput. Chem. Eng.*, tobe published.

[7] M. H. Nehrir, C. Wang, K. Strunz, H. Aki, R. Ramakumar, J. Bing, Z. Miao, and Z. Salameh, "A review of hybrid Renewable/Alternative energy systems for electric power generation: Configurations, control, and applications," *IEEE Trans. Sustain. Energy*, vol. **2**, no. 4, pp. 392–403, Oct. 2011.

[8] S. R. Vosen and J. O. Keller, "Hybrid energy storage systems for standal one electric power systems: Optimization of system performance and cost through control strategies," *Int. J. Hydrogen Energy*, vol. **24**, no. 12, pp. 1139–1156, Dec. 1999.

[9] M. Santarelli, M. Cali, and S. Macagno, "Design and analysis of standalone hydrogen energy systems with different renewable sources," *Int.J. Hydrogen Energy*, vol. **29**, no. 15, pp. 1571–1586, Dec. 2004.

[10] D. Nelson, M. Nehrir, and C. Wang, "Unit sizing and cost analysis of stand-alone hybrid wind/PV/fuel cell power generation systems," *Renew. Energy*, vol. **31**, no. 10, pp. 1641–1656, 2006.

[11] H. Yang, L. Lu, and W. Zhou, "A novel optimization sizing modelfor hybrid solar-wind power generation system," *Solar Energy*, vol. **81**, no. 1, pp. 76–84, Jan. 2007.

[12] J. L. Bernal-Agustín and R. Dufo-López, "Simulation and optimizationof stand-alone hybrid renewable energy systems," *Renew. Sustain. Energy Rev.*, vol. **13**, no. 8, pp. 2111–2118, Oct. 2009.

[13] R. Karki and R. Billinton, "Reliability/cost implications of PV and windenergy utilization in small isolated power systems," *IEEE Trans. Energy Convers.*, vol. **16**, no. 4, pp. 368–373, Dec. 2001.

[14] F. Valenciaga and P. F. Puleston, "Supervisor control for a stand-alonehybrid generation system using wind and photovoltaic energy," *IEEE Trans. Energy Convers.*, vol. **20**, no. 2, pp. 398–405, Jun. 2005.

[15] W. Qi, J. Liu, X. Chen, and P. D. Christofides, "Supervisory predictivecontrol of standalone wind/solar energy generation systems," *IEEE Trans. Control Syst. Technol.*, vol. **19**, no. 1, pp. 199–207, Jan. 2011.[16] C. Wang and M. H. Nehrir, "Power management of a stand-alonewind/photovoltaic/fuel-cell energy system," *IEEE Trans. Energy Convers.*,vol. 23, no. 3, pp. 957–967, Sep. 2008.

[17] S. Kim, J. H. Jeon, C. H. Cho, J. B. Ahn, and S. H. Kwon, "Dynamicmodeling and control of a grid-connected hybrid generation system withversatile power transfer," *IEEE Trans. Ind. Electron.*, vol. **55**, no. 4,pp. 1677–1688, Apr. 2008.

[18] Ø. Ulleberg, T. Nakken, and A. Eté, "The wind/hydrogen demonstrationsystem at utsira in norway: Evaluation of system performance usingoperational data and updated hydrogen energy system modeling tools,"*Int. J. Hydrogen Energy*, vol. **35**, no. 5, pp. 1841–1852, Mar. 2010.

[19] P. Hollmuller, J.-M. Joubert, B. Lachal, and K. Yvon, "Evaluation of a 5 kW*p* photovoltaic hydrogen production and storage installation fora residential home in Switzerland," *Int. J. Hydrogen Energy*, vol. **25**, no. 2, pp. 97–109, 2000.

[20] D. Ipsakis, S. Voutetakis, P. Seferlis, F. Stergiopoulos, and C. Elmasides,"Power management strategies for a stand-alone power system usingrenewable energy sources and hydrogen storage," *Int. J. Hydrogen Energy*, vol. **34**, no. 16, pp. 7081–7095, 2009.

[21] C. Ziogou, D. Ipsakis, C. Elmasides, F. Stergiopoulos, S. Papadopoulou, P. Seferlis, and S. Voutetakis, "Automation infrastructure and operation control strategy in a stand-alone power system based on renewable energy sources," *J. Power Sour.*, vol. **196**, pp. 9488–9499, Nov. 2011.

[22] Ø. Ulleberg, "Modeling of advanced alkaline electrolyzers: A systemsimulation approach," *Int. J. Hydrogen Energy*, vol. **28**, no. 1, pp. 21–33, Jan. 2003.

[23] Ø. Ulleberg, "The importance of control strategies in PV-hydrogen systems," *Solar Energy*, vol. **76**, nos. 1–3, pp. 323–329, Jan.–Feb. 2004.

[24] C. Wang, M. H. Nehrir, and S. R. Shaw, "Dynamic models and model validation for PEM fuel cells using electrical circuits," *IEEE Trans.Energy Convers.*, vol. **20**, no. 2, pp. 442–451, Jun. 2005.

[25] C. Wang, "Modeling and control of hybrid wind/photovoltaic/fuel cell distributed generation systems," Ph.D. dissertation, Monatana Univ.,Missoula, MT, USA, 2006.

[26] A. L. Dimeas and N. D. Hatziargyriou, "Operation of a multiagentsystem for microgrid control," *IEEE Trans. Power Syst.*, vol. **20**, no. 3,pp. 1447–1455, Aug. 2005.

[27] M. Trifkovic, M. Sheikhzadeh, K. Nigim, and P. Daoutidis, "Hierarchicalcontrol of a renewable hybrid energy system," in *Proc. 51st IEEE Annu.Conf. Decision Control*, Dec. 2012, pp. 6376–6381.

[28] B. C. Babu and K. B. Mohanty, "Doubly-fed induction generator forvariable speed wind energy conversion systems-modeling & simulation,"*Int. J. Comput. Electr. Eng.*, vol. **2**, no. 1, pp. 141–147, Feb. 2010.

[29] J. López, P. Sanchis, X. Roboam, and L. Marroyo, "Dynamic behaviorof the doubly fed induction generator during three-phase voltage dips,"*IEEE Trans. Energy Convers.*, vol. **22**, no. 3, pp. 709–717, Sep. 2007.

[30] W. Qi, J. Liu, and P. D. Christofides, "A distributed control frameworkfor smart grid development: Energy/water system optimal operationand electric grid integration," *J. Process. Control*, vol. **21**, no. 10, pp. 1504–1516, Dec. 2011.

[31] W. Leonhard, *Control of Electrical Drives*. New York, USA: Springer-Verlag, 2001.

[32] H. Bourdoucen and A. Gastli, "Tuning of PV array layout configurations for maximum power delivery," *Int. J. Electr. Inf. Eng.*, vol. **2**, no. 4.